Geoacoustic inversion on the New England Mud Patch using warping and dispersion curves of high-order modes

Julien Bonnel, Ying-Tsong Lin, Dimitrios Eleftherakis, John A. Goff, Stan Dosso, Ross Chapman, James H. Miller, and Gopu R. Potty

Citation: The Journal of the Acoustical Society of America **143**, EL405 (2018); doi: 10.1121/1.5039769

View online: https://doi.org/10.1121/1.5039769

View Table of Contents: http://asa.scitation.org/toc/jas/143/5

Published by the Acoustical Society of America

Geoacoustic inversion on the New England Mud Patch using warping and dispersion curves of high-order modes

Julien Bonnel,[1,a] Ying-Tsong Lin,[1] Dimitrios Eleftherakis,[2] John A. Goff,[3] Stan Dosso,[4] Ross Chapman,[4] James H. Miller,[5] and Gopu R. Potty[5]

[1]*Applied Ocean Physics and Engineering Department, Woods Hole Oceanographic Institution, Woods Hole, Massachusetts 02543, USA*

[2]*Laboratoire des Sciences et Techniques de l'Information, de la Communication Ecole Nationale Supérieure de Techniques Avancées, Bretagne, 29200 Brest, France*

[3]*Jackson School of Geosciences, The University of Texas at Austin, Austin, Texas 78712, USA*

[4]*School of Earth & Ocean Sciences, University of Victoria, Victoria, British Columbia V8W 2Y2, Canada*

[5]*Department of Ocean Engineering, University of Rhode Island, Narragansett, Rhode Island 02882, USA*

jbonnel@whoi.edu, ytlin@whoi.edu, dimitrios.eleftherakis@ensta-bretagne.fr, goff@ig.utexas.edu, sdosso@uvic.ca, chapman@uvic.ca, miller@uri.edu, gpotty@uri.edu

Abstract: This paper presents single receiver geoacoustic inversion of a combustive sound source signal, recorded during the 2017 Seabed Characterization Experiment on the New England Mud Patch, in an area where water depth is around 70 m. There are two important features in this study. First, it is shown that high-order modes can be resolved and estimated using warping (up to mode number 18 over the frequency band 20–440 Hz). However, it is not possible to determine mode numbers from the data, so that classical inversion methods that require mode identification cannot be applied. To solve this issue, an inversion algorithm that jointly estimates geoacoustic properties and identifies mode number is proposed. It is successfully applied on a range-dependent track, and provides a reliable range-average estimation of geoacoustic properties of the mud layer, an important feature of the seabed on the experimental area.

[DRB]

Date Received: March 27, 2018 **Date Accepted:** May 2, 2018

1. Introduction

Geoacoustic inversion in shallow water has historically been performed using array(s) of synchronous hydrophones. New methods have recently emerged, following technology developments and/or new signal processing algorithms. Among those, a non-linear signal processing method called warping has opened the door for single receiver low-frequency geoacoustic inversion (Bonnel *et al.*, 2013), which has gradually been adopted by the community (Ballard *et al.*, 2014; Duan *et al.*, 2016; Petrov, 2014; Warner *et al.*, 2015).

Warping inversion is adapted to the context of low-frequency impulsive sources in shallow water. In this case, the pressure field is described by a set of modes that propagates dispersively. Each mode possesses its unique characteristics in the time-frequency (TF) domain, which can be described by modal dispersion curves. These curves can be estimated by the warping technique, and used as data for inversion algorithms. To date, such algorithms have required mode identification, i.e., one must know the mode number associated with each dispersion curve.

The problem of mode identification using a single receiver has not been considered previously in the literature. The usual assumption is that if there are M modes, they represent modes 1 to M. This holds true if the number of modes resolved is relatively small, which is the case in the references quoted above, where $M < 5$. However, this paper demonstrates with measured data that warping enables the resolution and estimation of high-order modes (here, up to mode number 18 over the frequency band 20–440 Hz with water depth $\simeq 70$ m). In this case, the former simple assumption on mode identification is not necessarily valid. A new inversion scheme that does not require mode identification is thus proposed.

[a]Author to whom correspondence should be addressed.

Another feature of this study is that the considered source/receiver track is range-dependent. Prior information about the seabed layering is known through two-way travel times (twtts) obtained using a chirp sonar survey. The twtts will be used as an input for a fully non-linear inversion. In a similar context, Ballard *et al.* (2010) used twtt information to perform a linearized inversion based on wavenumbers. TF dispersion curve inversion in a range-dependent context has been proposed by some researches, including Petrov (2014) and Wan *et al.* (2018), but less than five modes were used, and mode numbers were known *a priori*. This study differs from previous inversion work because it uses TF modal dispersion from high-order modes.

The method described above is applied to data collected during the Seabed Characterization Experiment (SBCEX) in the spring of 2017. The experimental area is the New England Mud Patch (Bothner *et al.*, 1981; Twichell *et al.*, 1981), located 110 km south of Cape Cod, MA. One of the seabed characteristics is a top layer of fine grained sediments (i.e., mud) whose geoacoustic properties were unknown before SBCEX. Our method provides a reliable estimate of the mud characteristics.

2. Data description

There were a variety of acoustic sources and receivers deployed during SBCEX. This paper considers a Combustive Sound Source (CSS) signal transmitted on March 13 at 21:53 UTC. The source position was 40.478 N; 70.524 W and the source depth is about $z_s = 12.5$ m. The CSS signal is known to be a high-intensity low-frequency pulse, followed by several weaker bubble pulses (McNeese *et al.*, 2010). The source signature was measured during the experiment using a monitor hydrophone 1 m from the CSS (hard-mounted to the CSS deployment frame).

The acoustic field is recorded $r \simeq 4.8$ km away from the source on a bottom moored acoustic receiver located at 40.499 N; 70.475 W. Although the receiver has four channels, a single hydrophone 0.65 m above the seafloor is used is this study. The bathymetry along the track is range-dependent (Fig. 1). The sub-bottom layering along the profile was derived from an interpretation of chirp acoustic reflection data collected in 2015 (Goff *et al.*, 2016). Chirp profiles were densely sampled (≃250 m line spacing), allowing for interpolation and gridding of interpreted reflection horizons across the survey area. The individual horizons shown in Fig. 1 represent a track-line sampling of these gridded surfaces between the source and receiver locations.

The water sound speed profile was measured near the source and near the receiver during the experiment. It is relatively constant and barely presents spatial variability. It can be modeled as a constant gradient from 1464 m/s at the surface to 1465 m/s at the seabed (note that using this model, the sound speed gradient changes slightly along the track, as water depth changes).

The received signal is shown in Fig. 2(a), and its spectrogram (after low-pass filtering) is shown in Fig. 2(b).

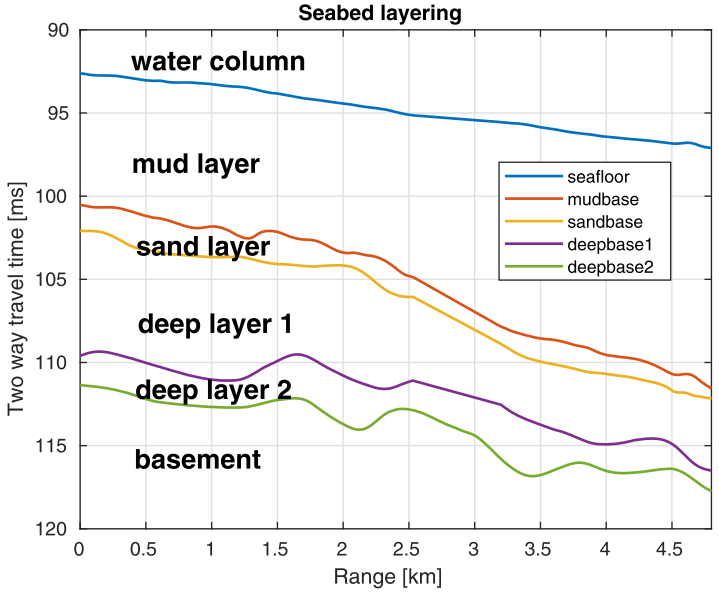

Fig. 1. (Color online) Seabed layering along the considered track, given in twtt (ms). The source and receiver are, respectively, at range $r = 0$ and $r = 4.8$ km.

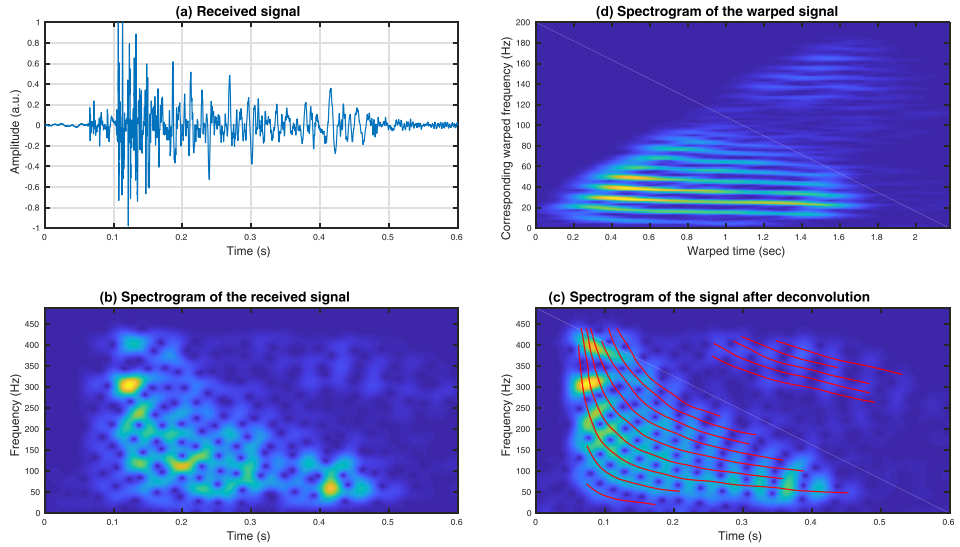

Fig. 2. (Color online) (a) Received signal (amplitude is normalized and given in arbitrary units). (b) Spectrogram of the received signal. (c) Spectrogram of the signal after source deconvolution, and estimated dispersion curves. (d) Spectrogram of the signal after source deconvolution and warping.

3. Modal propagation and single receiver context

In our context (low-frequency acoustic waves in shallow water), propagation is conveniently described by normal-mode theory. In a waveguide with smooth range-dependent variations, considering a broadband signal emitted at depth z_s, the received pressure field Y at depth z_r after propagation over a range r is given through adiabatic modes by (Jensen *et al.*, 2011)

$$Y(r,f) \simeq AS(f) \sum_{m=1}^{N} \Psi_m(f,z_s)\Psi_m(f,z_r) \frac{e^{j\int_0^r k_{rm}(r',f)\,dr'}}{\sqrt{\int_0^r k_{rm}(r',f)\,dr'}}, \tag{1}$$

where N is the number of propagating modes, $k_{rm}(r',f)$ is the mode m horizontal wavenumber at range r', $\Psi_m(f,z_s)$ is the mode m depth function for the environment at the source position, and $\Psi_m(f,z_r)$ is the modal m depth function for the environment at the receiver position. The quantity $S(f)$ is the source spectrum and A is a constant factor.

When considered in the TF domain, the received field is concentrated around the dispersion curves. For an impulse emitted at time t_s, the dispersion curve of mode m follows, e.g., Bonnel *et al.* (2013),

$$t_m(r,f) = \frac{r}{v_{gm}(r,f)} + t_s, \tag{2}$$

where $v_{gm}(r,f) = r/\int_0^r [dr'/v_{gm}(r',f)]$ is the adiabatic approximation of the group velocity at range r.

4. Inversion scheme

4.1 Source deconvolution

Source deconvolution is usually ignored when dealing with impulsive source geoacoustic inversion, because the source is assumed to be a single perfect pulse, so that the received signal approximates the waveguide impulse response [e.g., Bonnel *et al.* (2013)]. It nonetheless has been suggested in Duan *et al.* (2016) that, because of the bubble pulses, the experimental source cannot be considered as an impulse. It was further shown that source deconvolution enables the use of a wider frequency band on which modes can be resolved.

In our case, the source signal $S(f)$ was measured during the experiment (see Sec. 2), so that source deconvolution is straightforward. Here, a classical deconvolution method is used (Clayton and Wiggins, 1976). The received signal after deconvolution is

$$Y_{\text{deconv}}(f) = \frac{Y(f)S^*(f)}{\max\left\{|S(f)|^2, \epsilon\right\}}, \tag{3}$$

with ϵ empirically chosen as $\epsilon = 0.01\max\{|S(f)|^2\}$.

As an illustration, Fig. 2(b) shows the spectrogram of the received signal, in which it is barely possible to distinguish the modes. Figure 2(c) shows the spectrogram of the signal after source deconvolution. The modes still interfere with each other, because the range is relatively short. However, the spectrogram is clearer. Although the measured $S(f)$ may be contaminated by surface and/or ship hull reflection(s), the deconvolution result appears to be an improvement. It is at least good enough to estimate the dispersion curves with warping, as will be described below.

4.2 Dispersion curve estimation

After source deconvolution, dispersion curves can be estimated using warping, which is a physics-based non-linear re-sampling of the signal. It is an invertible transform, so the warped signal can be unwarped. When warping is applied properly, the spectrogram of the warped signal shows the modes as nearly horizontal tones. The modal dispersion curves can then be estimated using standard TF filtering and unwarping [see Bonnel *et al.* (2013) for more details].

The spectrogram of the warped signal is shown in Fig. 2(d), which shows that the warped modes are nearly horizontal, and nicely separated. Such a result was impossible to obtain without source deconvolution, which further confirms the results obtained in Duan *et al.* (2016). It also requires a fine tuning of warping time origin, as detailed in Bonnel *et al.* (2017).

The final result of the estimation scheme is shown in Fig. 2(c), where the estimated dispersion curves are superimposed in red on the spectrogram. One can note a gap between low-order modes and high-order modes, both in Figs. 2(c) and 2(d). While the first 9 modes are modes 1 to 9 with little doubt, it is impossible to identify the last 5 high-order modes. This requires a new inversion scheme, which does not require prior knowledge of mode numbers.

4.3 Inversion method

In this context, we denote $\hat{t}_m(f_n)$ to be the mth estimated dispersion curve at frequency f_n, and $N(m)$ the number of frequencies for this mode. The quantities $\hat{t}_m(f_n)$ are thus the data to be inverted, and we suppose that M_d modes are available. Note that because mode identification is not available, $\hat{t}_m(f_n)$ does not necessarily correspond to mode m, and the M_d data modes do not necessarily correspond to mode numbers 1 to M_d.

We further denote $t_p(f_n, \boldsymbol{\theta})$ the replica (i.e., predicted) dispersion curve for mode p, as simulated in an environment parametrized by $\boldsymbol{\theta}$. For a given $\boldsymbol{\theta}$, M_r replicas are simulated. Inversion is then carried out as usual, comparing data $\hat{t}_m(f_n)$ to replicas $t_p(f_n, \boldsymbol{\theta})$. However, data mode m is compared to all the replicas ($p \in [1, M_r]$), and the misfit is computed with the nearest replica. Mathematically

$$[\hat{\theta}] = \underset{\boldsymbol{\theta}}{\text{argmin}} \left\{ \sum_{m=1}^{M_d} \sum_{n=1}^{N(m)} \left[\hat{t}_m(f_n) - t_{m_0(\boldsymbol{\theta})}(f_n, \boldsymbol{\theta})\right]^2 \right\}, \tag{4}$$

with

$$m_0(\boldsymbol{\theta}) = \underset{p}{\text{argmin}} \left\{ \sum_{n=1}^{N(m)} \left[\hat{t}_m(f_n) - t_p(f_n, \boldsymbol{\theta})\right]^2 \right\}. \tag{5}$$

Note that M_r must be significantly larger than M_d. This ensures that the replicas span enough modes to include the data mode numbers, or in other words, this allows $m_0(\boldsymbol{\theta}) = m$ for a well-chosen $\boldsymbol{\theta}$.

4.4 Application to the SBCEX context

The inversion scheme presented above is applied to the SBCEX data. The water sound-speed profile and the seabed layering (see Sec. 2) are used as prior information for the inversion. Thirteen parameters are then inverted (see Table 1):

- mud: sound speed at the top of the layer $c_{\text{mud}}^{\text{TOP}}$, sound speed at the bottom of the mud layer $c_{\text{mud}}^{\text{BOT}}$, and constant density ρ_{mud},
- other layers (including basement): constant sound speed c_i and density ρ_i,
- range r and time shift dt to account for uncertainty in source explosion time.

Table 1. Summary of inversion results.

Parameter	Unit	Search bounds	Estimated value
$c_{\text{mud}}^{\text{TOP}}$	m/s	[1440; 1600]	1464
$c_{\text{mud}}^{\text{BOT}}$	m/s per m	[1440; 1800]	1540
c_{sand}	m/s	[1440; 2000]	1745
c_{deep1}	m/s	[1440; 2000]	1775
c_{deep2}	m/s	[1440; 2000]	1625
c_{bas}	m/s	[1500; 3000]	1859
ρ_{mud}	—	[1.0; 2.0]	1.33
ρ_{sand}	—	[1.0; 2.0]	1.86
ρ_{deep1}	—	[1.0; 2.0]	1.57
ρ_{deep2}	—	[1.0; 2.0]	1.05
ρ_{bas}	—	[1.5; 3.0]	1.85
dt	s	[−3.4; −3.1]	-3.275
r	km	[4.75; 4.85]	4.80

The modal replicas are computed using the normal-mode code ORCA (Westwood *et al.*, 1996). To do so, the range-dependent track is divided into 100 m range-independent sections, and $M_r = 25$ range-dependent replicas are computed. Minimization of Eq. (4) is done using an Adaptive Simplex Simulated Annealing algorithm (Dosso *et al.*, 2001), and minimization of Eq. (5) is done using an exhaustive search over the M_r replicas. The search space for each parameter is listed in Table 1.

The sound speed gradient in the mud layer can be locally defined as $g_{\text{mud}} = c_{\text{mud}}^{\text{TOP}} - c_{\text{mud}}^{\text{BOT}}/h_{\text{mud}}$, with h_{mud} the local mud thickness. Because h_{mud} varies along the track, so does g_{mud}. Note that the modeled speed profile in the mud is $1/c^2$ linear, so that the definition of the gradient is not mathematically correct, but nonetheless useful to summarize mud properties. For each $\boldsymbol{\theta}$, the true $1/c^2$-profile has been used to locally adapt layer thickness based on $c_{\text{mud}}^{\text{TOP}}$, $c_{\text{mud}}^{\text{BOT}}$, and the twtt information.

5. Results and discussion

Inversion results are shown in Fig. 3 and summarized in Table 1. Predicted modes are compared with data in Fig. 4. The excellent match demonstrates the success of the inversion. It is also interesting to note that range is estimated within two dozen meters of the ground truth (obtained with Global Positioning System).

The geoacoustic estimates of the mud layer are consistent with what is known in the area. The estimated $c_{\text{mud}}^{\text{TOP}}$ is 1464 m/s, which leads to a 0.999 sound speed ratio at the water/mud interface. The min/mean/max thickness of the mud layer along the track are 7.9/10.6/14.7 ms (twtt). Using the estimated $c_{\text{mud}}^{\text{TOP}}$ and $c_{\text{mud}}^{\text{BOT}}$, the min/mean/max thicknesses are 6.0/8.0/11.1 m, so that the min/mean/max sound speed gradients in the mud are 6.75/9.33/12.56 m/s per m. Such gradient values are higher than expected using propagation models in fine grained sediments. However, they are consistent with

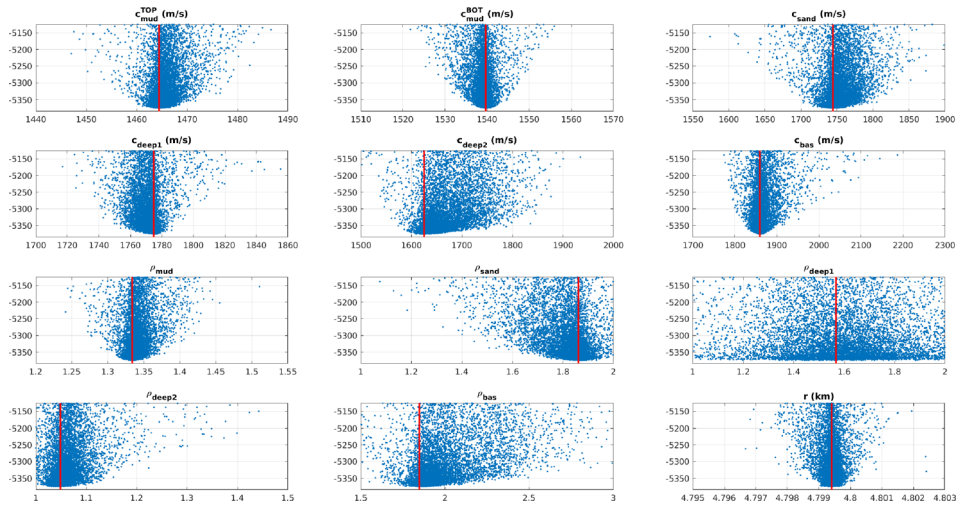

Fig. 3. (Color online) Scatter plots: the dots represent the mismatch as a function of parameter values during the inversion. The vertical line gives the final estimated value of each parameter. Results are not shown for dt for layout convenience.

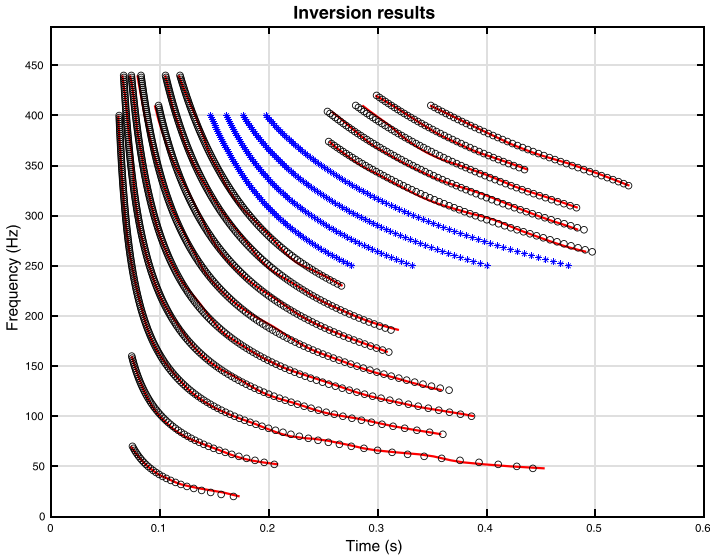

Fig. 4. (Color online) Dispersion curves as estimated from the data with warping (lines) and predicted after inversion (circles). The predicted dispersion curves for modes 10 to 13 (absent in the data) are also shown (crosses).

most of the preliminary acoustic inversion results obtained in this area.[1] In particular, such a high gradient has also been found by another independent full-waveform inversion on the same track (Lin *et al.*, 2017), as well as by dispersion curve inversion using 4 modes from 10 to 80 Hz on another track (Wan *et al.*, 2018). Inversion results for a deeper layer may be questionable, as there is no means to verify them. In particular, the speed in the second deep layer is too low to be realistic, and so is the density. It is nonetheless logical to have a poor estimate in this layer because of its small thickness with respect to the wavelengths in the sound signal. Actually, the model is likely over parameterized, and the thin deep layer 2 could probably be excluded from the seabed model. It has been kept here because it barely impacts mud geoacoustic estimates, and because it allows easy comparison with other work in the same area, such as Wan *et al.* (2018). A careful study of the data capacities to resolve layers is out of the scope for such a letter, but is of particular interest for future studies, particularly when considering a high number of modes whose depth resolution varies.

The inversion result demonstrates that the data contains modes 1 to 9 and 14 to 18 (i.e., modes 10 to 13 are missing). This is likely due to insufficient modal excitations because of the source/receiver depth configuration. However, of particular interest here is the fact that the proposed method allows inversion without mode identification. The price to pay for an unknown mode number is that range and explosion time must be estimated accurately in the inversion, otherwise there may be a wrong match in Eq. (5).

6. Conclusion

This paper presented single receiver geoacoustic inversion of a CSS signal, recorded during the 2017 SBCEX on the New England Mud Patch. A careful combination of source deconvolution and warping allowed the resolution and estimation of 14 modes. The estimated modal pattern showed a gap in between modes, so that mode identification was not possible from the data. To circumvent this issue, a new inversion algorithm was proposed. It was successfully applied on a range-dependent track, and provided a reliable estimate of the mud geoacoustic properties. In particular, the sound speed ratio at the mud/water interface is about 1. Also, the sound speed in the mud has a strong positive gradient, whose mean value is nearly 10 m/s per m.

Acknowledgments

This research was supported by the Office of Naval Research and the Office of Naval Research Global. The UTIG contribution number is 3270. The authors thank D. Knobles and P. Wilson for leading SBCEX and for providing the CSS source signal.

References and links

[1]These results were presented at a SBCEX special session during the 2017 ASA meeting in New Orleans. As far as we know, Wan *et al.* (2018) is the single peer-reviewed paper published on SBCEX at the time this letter is written.

Ballard, M., Becker, K., and Goff, J. (**2010**). "Geoacoustic inversion for the New Jersey shelf: 3-D sediment model," IEEE J. Ocean. Eng. **35**(1), 28–42.

Ballard, M. S., Frisk, G. V., and Becker, K. M. (**2014**). "Estimates of the temporal and spatial variability of ocean sound speed on the New Jersey shelf," J. Acoust. Soc. Am. **135**(6), 3316–3326.

Bonnel, J., Caporale, S., and Thode, A. (**2017**). "Waveguide mode amplitude estimation using warping and phase compensation," J. Acoust. Soc. Am. **141**(3), 2243–2255.

Bonnel, J., Dosso, S., and Chapman, R. (**2013**). "Bayesian geoacoustic inversion of single hydrophone light bulb data using warping dispersion analysis," J. Acoust. Soc. Am. **134**, 120–130.

Bothner, M. H., Spiker, E., Johnson, P., Rendigs, R., and Aruscavage, P. (**1981**). "Geochemical evidence for modern sediment accumulation on the continental shelf off southern New England," J. Sedimentary Res. **51**(1), 281–292, available at http://archives.datapages.com/data/sepm/journals/v51-54/data/.

Clayton, R. W., and Wiggins, R. A. (**1976**). "Source shape estimation and deconvolution of teleseismic bodywaves," Geophys. J. Int. **47**(1), 151–177.

Dosso, S., Wilmut, M., and Lapinski, A. (**2001**). "An adaptive-hybrid algorithm for geoacoustic inversion," IEEE J. Ocean. Eng. **26**(3), 324–336.

Duan, R., Chapman, N. R., Yang, K., and Ma, Y. (**2016**). "Sequential inversion of modal data for sound attenuation in sediment at the New Jersey Shelf," J. Acoust. Soc. Am. **139**(1), 70–84.

Goff, J., Chaytor, J., Reed, A., Liu, S., Wilson, P., and Knobles, D. (**2016**). "The coarse-to fine-grained boundary beneath the New England mud patch: Evidence from seismic and core data for an abrupt post-transgressive change in hydrologic regime on the continental shelf," in *AGU Fall Meeting Abstracts*.

Jensen, F., Kuperman, W., Porter, M., and Schmidt, H. (**2011**). *Computational Ocean Acoustics*, 2nd ed. (AIP, New York).

Lin, Y.-T., Duda, T. F., Newhall, A., and Gawarkiewicz, G. (**2017**). "Surface wave effects on bottom geoacoustic inversions," J. Acoust. Soc. Am. **142**(4), 2590.

McNeese, A. R., Sagers, J. D., Wilson, P. S., and Knobles, D. P. (**2010**). "An investigation of the combustive sound source," Proc. Mtgs. Acoust. **9**, 005002.

Petrov, P. (**2014**). "A method for single-hydrophone geoacoustic inversion based on the modal group velocities estimation: Application to a waveguide with inhomogeneous bottom relief," in *Days on Diffraction* (*DD*), IEEE, pp. 186–191, available at http://archives.datapages.com/data/sepm/journals/v51-54/data/051/.

Twichell, D. C., McClennen, C. E., and Butman, B. (**1981**). "Morphology and processes associated with the accumulation of the fine-grained sediment deposit on the southern New England shelf," J. Sedimentary Res. **51**(1), 269–280.

Wan, L., Badiey, M., Knobles, D. P., and Wilson, P. S. (**2018**). "The airy phase of explosive sounds in shallow water," J. Acoust. Soc. Am. **143**(3), EL199–EL205.

Warner, G. A., Dosso, S. E., Dettmer, J., and Hannay, D. E. (**2015**). "Bayesian environmental inversion of airgun modal dispersion using a single hydrophone in the Chukchi Sea," J. Acoust. Soc. Am. **137**(4), 2361–2362.

Westwood, E. K., Tindle, C., and Chapman, N. (**1996**). "A normal mode model for acousto-elastic ocean environments," J. Acoust. Soc. Am. **100**(6), 3631–3645.